Journal of Power Sources 189 (2009) 864–868

Contents lists available at ScienceDirect

Journal of Power Sources

journal homepage: www.elsevier.com/locate/jpowsour

Short communication

The electrochemical properties of copper sulfide as cathode material for rechargeable sodium cell at room temperature

Jong-Seon Kim[a], Dong-Yeon Kim[a], Gyu-Bong Cho[a], Tae-Hyun Nam[a], Ki-Won Kim[a], Ho-Suk Ryu[a], Jou-Hyeon Ahn[b], Hyo-Jun Ahn[a,*]

[a] School of Materials Science and Engineering, i-Cube Center, ERI, Gyeonsang National University, Jinju, South Korea
[b] Department of Biological and Chemical Engineering, Gyeonsang National University, Jinju, South Korea

ARTICLE INFO

Article history:
Received 29 June 2008
Received in revised form 15 October 2008
Accepted 15 October 2008
Available online 1 November 2008

Keywords:
Copper sulfide
Sodium anode
Sodium rechargeable battery
Na/Cu_2S

ABSTRACT

The sodium/copper sulfide (Na/Cu_2S) rechargeable batteries are investigated using 1 M $NaCF_3SO_3$-TEGDME liquid electrolyte at room temperature. The first discharge curve of Na/Cu_2S cells shows a slope shape without plateaus potential region. The first discharge capacity is 294 mAh g^{-1} and decreases to 220 mAh g^{-1} after 20 cycles. The discharge process can be explained by intercalation of sodium into Cu_2S phase without phase separation of Cu_2S.

1. Introduction

The batteries are important power sources for portable electric devices, electric vehicles (EVs), hybrid electric vehicles (HEVs) and electricity storages [1,2]. Especially, large-scale batteries for HEVs and electricity storage have been focused on properties such as high energy density, high power density, high safety and low material cost. Na/S, Ni/Cd, Ni/MH, lead acid and Li-ion batteries have been intensively investigated [3–7].

A sodium/sulfur (Na/S) battery has been one of the possible candidates for electricity storage due to high theoretical specific energy density of 760 Wh kg^{-1}, long cyclic life and low material costs. However, one of the severe problems of the sodium/sulfur battery is its high operating temperature above 300 °C, which could induce explosions, corrosion and power consumption to maintain heating at its operating temperature [8,9]. In order to decrease operating temperature of sodium batteries, many materials have been studied as anodes or cathodes of the sodium battery [10–13]. Sodium/metal sulfides (Na/Ni_3S_2, Na/FeS_2) as well as sodium/sulfur batteries showed good electrochemical properties at room temperature [1,14,15]. Especially, copper sulfide (Cu_2S) can be one of the potential candidates for cathode materials of sodium batteries. Cu_2S has high theoretical capacity and low material cost due to existence of chalcocite (Cu_2S) ore in nature. Although the Na/Cu_2S cell could be a potential candidate for large-scale battery, there was no study about the Na/Cu_2S cell at room temperature.

In this paper, the Na/Cu_2S cell was prepared and the electrochemical properties of the cell were studied at room temperature. In order to understand the discharge mechanism of Na/Cu_2S cells, the electrodes after the first cycle were analyzed by SEM, XRD, TEM, and EDS tools.

2. Experimental

Copper sulfide (Cu_2S, −325 mesh) was bought from Aldrich Corporation. In order to decrease the particle size, a ball-milling was executed by a planetary system (FRITSCH. Co.) for 1.5 h. Super-P was used as a conductive agent and poly ethylene oxide (PEO, $(-CH_2CH_2O)_n$, Aldrich) was used as a binder.

A Cu_2S electrode was prepared from a suspension of 60 wt% ball-milled Cu_2S, 20 wt% Super-P, and 20 wt% PEO in acetonitrile. The suspension was mixed for 3 h by attrition ball-mill and then cast onto Al foil. The suspension was dried in an oven at 60 °C for 24 h and then at 50 °C for 5 h under a vacuum atmosphere to remove any residual solvent and volatile impurities. The dried cathode film was cut into discs of 1.0 cm diameter. The sodium anode was prepared by cutting a sodium ingot in an argon gas atmosphere. The liquid electrolyte was 1 M sodium trifluoromethanesulfonate

* Corresponding author. Tel.: +82 55 751 5308; fax: +82 55 759 1745.
E-mail address: ahj@gnu.ac.kr (H.-J. Ahn).

0378-7753/$ – see front matter © 2008 Elsevier B.V. All rights reserved.
doi:10.1016/j.jpowsour.2008.10.057

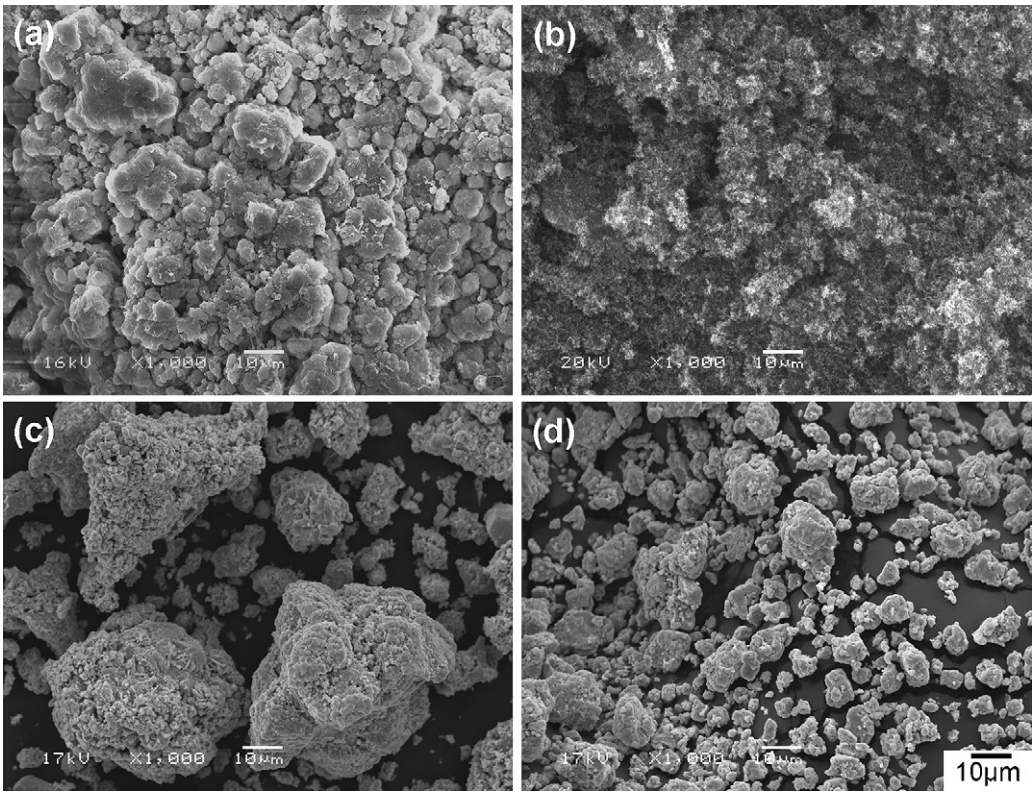

Fig. 1. SEM morphologies of raw materials: (a) PEO, (b) carbon, (c) raw Cu_2S and (d) Cu_2S powder after ball-milling for 1.5 h.

($NaCF_3SO_3$, Aldrich) salt in tetra ethylene glycol dimethyl ether (TEGDME, Aldrich Chem. Co.).

The electrochemical tests were performed by WBCS 3000 Battery Tester (WonA Tech) at room temperature. The cell was kept to equilibrate electrochemically for two hours and then a galvanostatic test was carried out between 0.4 and 2.6 V in a constant current density of 50 mA g^{-1}. The crystal structure of the Cu_2S electrode was investigated using an X-ray diffractometer and transmission electron microscopy (TEM). Scanning electron microscopy was used to observe changes in the surface morphology of cathodes. Elemental mapping of Cu_2S electrodes was performed using energy dispersive spectrometer (EDS).

3. Results and discussion

Fig. 1 shows SEM morphologies for raw materials of the Cu_2S cathode. PEO particles are agglomerated with small particles. Super-P particles have submicron diameter and very large surface areas. Various particle sizes of Cu_2S powders (Aldrich, −325 mesh) are observed and some of them have above 50 μm diameter. The particle size of Cu_2S powders decrease below 15 μm by a ball-milling for 1.5 h.

Fig. 2 shows the X-ray diffraction patterns of the raw materials. The sharp peaks of PEO indicate a crystalline structure. Super-P shows one broad peak which can be explained by a nanocrystalline structure. The XRD patterns of the purchased Cu_2S powders are coincided with the monoclinic structure of Cu_2S. After a ball-milling process, monoclinic structure is still maintained. However, peak intensity decreases and the peak width increases, which might result from internal strain by ball-milling.

Fig. 3 shows discharge–charge and cycle voltammogram (CV) curves of the Na/Cu_2S cell. The discharge curve represents a slope-shape profile without distinct plateau potential regions. The first discharge capacity is 294 mAh g^{-1} that implies the intercalation of 1.75 sodium atom into the Cu_2S. The first charge curve shows the two plateaus at 1.64 and 2.14 V. And the first charge capacity is 270 mAh g^{-1}, which means 91% coulombic efficiency. The CV test was carried out in the potential sweep rate of 0.1 mV s^{-1} at the voltage range from 0.4 to 2.6 V versus Na/Na^+ at ambient temperature. The several oxidation peaks take place at the region from 0.9 to 2.0 V, and two reduction peaks appear at 1.85 and 2.20 V. The CV curve coincided with charge–discharge curve.

Fig. 4 shows the changes of SEM images of Cu_2S electrodes after charge and discharge. The original Cu_2S electrode shows a homogenous mixture of the Cu_2S, PEO and Super-P powders. After discharge reaction, the surface of Cu_2S electrode is covered by a dense film

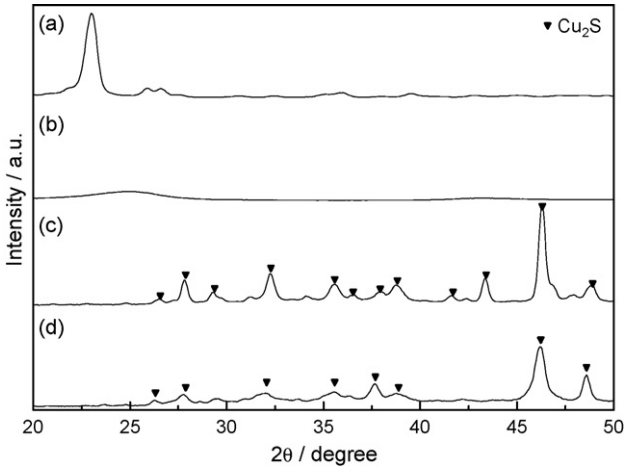

Fig. 2. XRD patterns of raw materials: (a) PEO, (b) carbon, (c) raw Cu_2S and (d) Cu_2S after ball-milling for 1.5 h.

which is similar to sodium/metal sulfide cells (Na/Ni_3S_2, Na/FeS_2) [14,15]. The surface of charged electrode shows a shape similar to the original electrode.

Fig. 5 shows elemental mapping on SEM images of Cu_2S electrodes. The bright spots correspond to the presence of the sulfur, copper and sodium elements, respectively. After discharging, copper, sulfur and sodium are detected. The copper and sulfur come from an original Cu_2S phase and the sodium is detected due to intercalation of sodium into the Cu_2S electrode during discharging. After charging, sodium as well as sulfur and copper are detected. Although the sodium must return to the sodium anode from Cu_2S cathode during charging, sodium element still remains in the Cu_2S electrode. This might be related to the difference between the discharge capacity and charge capacity shown in Fig. 3.

In order to investigate the phase change during the first cycling, the XRD, TEM and SAED (selected area electron diffraction) pattern are investigated. Fig. 6 shows the changes of XRD patterns after discharging and charging. The XRD pattern of the original Cu_2S electrode shows Cu_2S, PEO and Al phase. Since the Cu_2S electrode is composed of Cu_2S, PEO and Super-P, Cu_2S and PEO phases are observed. Al peaks should come from an Al current collector. After discharging, we cannot find any peaks related to copper or sodium sulfides. The discharge process of Na/Cu_2S cell cannot be explained by the phase separation of Cu_2S by sodium ($Na + Cu_2S \rightarrow Na_2S + Cu$). The discharged electrode shows only Cu_2S phase, but the peak positions slightly shift. From XRD pattern, we can find the increase of

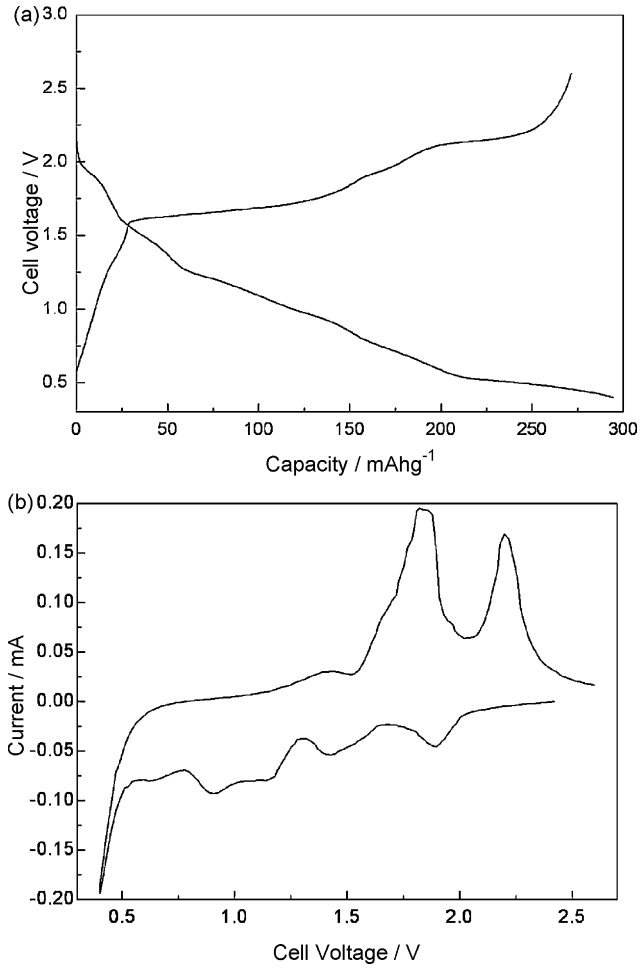

Fig. 3. The discharge–charge and CV curves of the Na/Cu_2S cell at room temperature: (a) first discharge–charge curve with 50 mA g^{-1} and (b) CV curve of Cu_2S vs. Na.

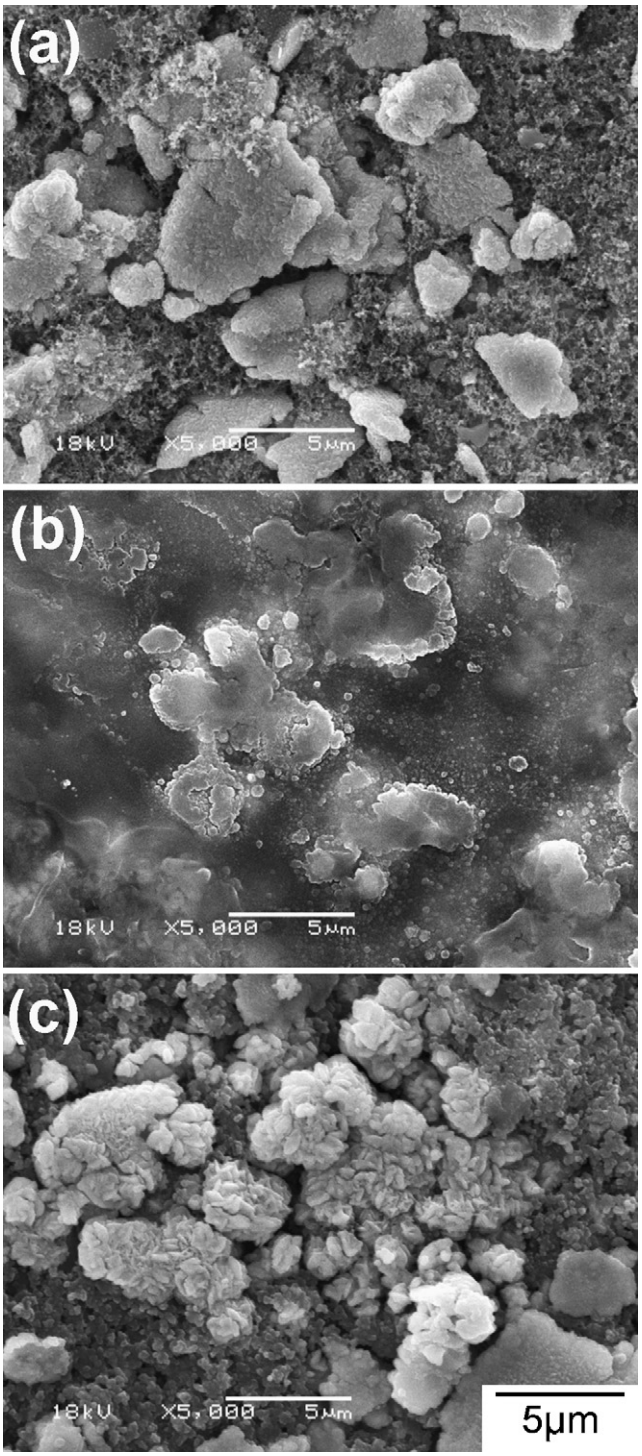

Fig. 4. The change in SEM morphologies of Cu_2S electrodes: (a) original electrode, (b) after discharge and (c) after charge.

unit cell volume of Cu_2S electrode, which may originate from the intercalation of sodium into Cu_2S. The charged electrode shows the peak shift of Cu_2S phase by decrease of unit cell volume due to deintercalation of sodium.

The structure of Cu_2S is confirmed by the TEM image and SAED measurement.

Fig. 7 shows the TEM image and SAED pattern of discharged Cu_2S electrode. Cu_2S powder seems to be composed of a lot of nanometer-sized particles. The SAED pattern exhibits the rings

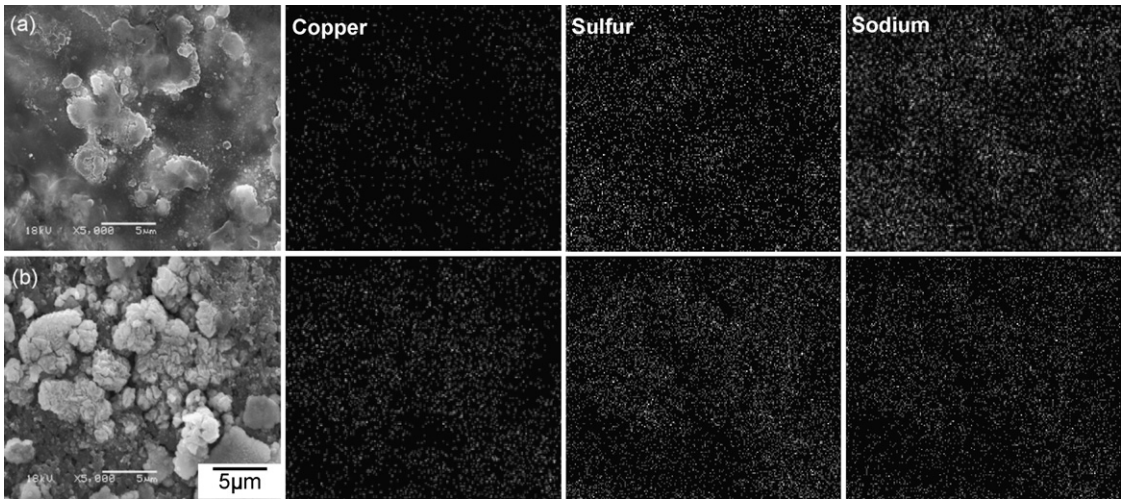

Fig. 5. EDS mapping patterns of copper sulfide electrodes: (a) after first discharge and (b) after first charge.

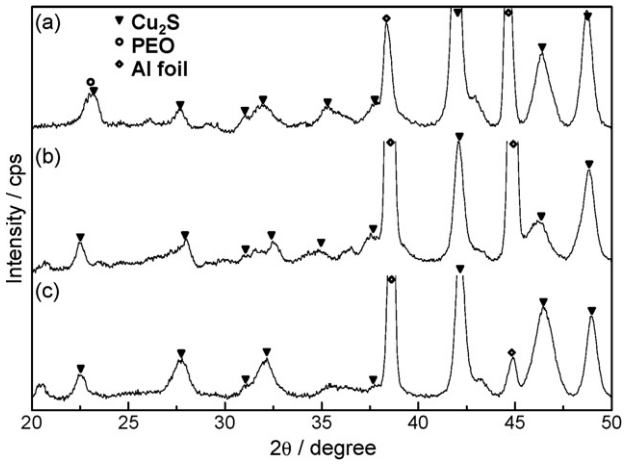

Fig. 6. XRD patterns of Cu_2S electrodes: (a) original, (b) after first discharge and (c) after first charge.

made up of discrete spots which can be interpreted as the nano-sized polycrystalline. All *d*-spacings derived from SAED spectra could not match with Cu or Na_2S but assign to Cu_2S. SAED spectrum shows the same result as XRD results shown in Fig. 6.

From the data, we can suggest the discharge and charge mechanism.

From EDS data shown in Fig. 5, the discharged Cu_2S electrode has sodium element. XRD and TEM data represent the existence of Cu_2S phase with large unit cell volume. Thus, the discharge process of Cu_2S can be explained by intercalation sodium into Cu_2S phase like Eq. (1).

$$Cu_2S + xNa \rightarrow Na_xCu_2S (x < 2) \quad (1)$$

EDS data show the existence of sodium element in the charged cathode. However, XRD data shows only Cu_2S phase without sodium phase. We think that sodium can exist as Na_yCu_2S. Therefore the following reactions may be possible during charging.

$$Na_xCu_2S \rightarrow Na_{x-y}Cu_2S + yNa (x, y < 2) \quad (2)$$

Fig. 8 shows the changes of coulombic efficiency, capacity of charge and discharge. The capacity decreases drastically by the 4th

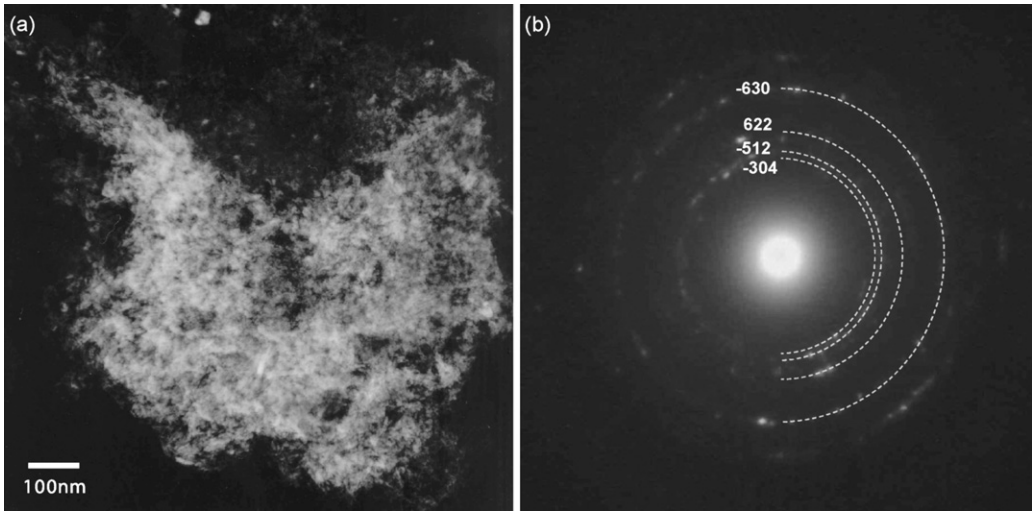

Fig. 7. TEM image and SAED pattern of Cu_2S electrode after 1st discharge: (a) TEM image and (b) SAED pattern.

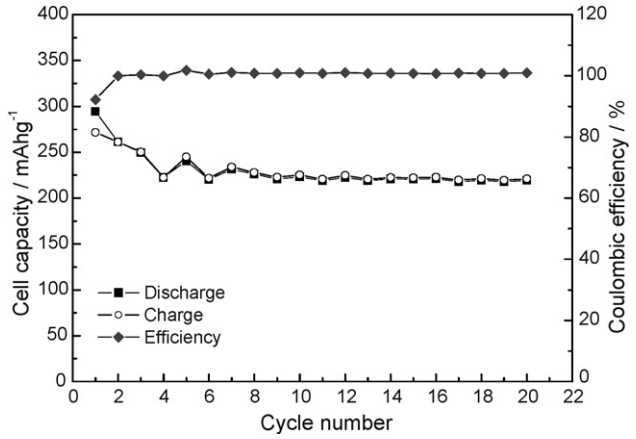

Fig. 8. Coulombic efficiency and change of a charge and discharge capacities vs. the cycle number of Na/Cu_2S cells.

cycle, but the capacity does not change after the 4th cycle. The first discharge capacity is 294 mAh g^{-1} and decreases to 261 mAh g^{-1} after 20 cycles. The discharge capacity of Initial coulombic efficiency is 92%, which may relate to remaining sodium after the first charge. After the 2nd cycle, the coulombic efficiency maintains 100% until 20 cycles, which can be considered as reversible reaction since the 2nd cycle. In previous works, Park et al. [12] reported that the room temperature Na/S cell decreased to 9% of initial capacity after 20 cycles. Although the theoretical capacity of Na/Cu_2S cells is lower than Na/S cells, cycle performance is better than room temperature Na/S cell. However, it is necessary to improve long-term cycle stability and rate capability.

4. Conclusions

The Na/Cu_2S cell has a sloping shape without distinct plateaus and the first discharge capacity of 294 mAh g^{-1} at room temperature. The discharge capacity decreases to 220 mAh g^{-1} after the 20th cycle. Na/Cu_2S cell shows high coulombic efficiency during cycling. From results of XRD, EDS, TEM analyses, the discharge process can be explained by intercalation of sodium into Cu_2S phase without phase separation of Cu_2S.

$$Cu_2S + xNa \leftrightarrow Na_xCu_2S(x < 2)$$

Acknowledgements

This research was supported by the MKE (Ministry of Knowledge Economy), Korea, under the ITRC (Information Technology Research Center) support program supervised by IITA (Institute of Information Technology Assessment) and Pioneer Research Project by MEST (Ministry of Education, Science and Technology).

References

[1] T.B. Kim, W.H. Jung, H.S. Ryu, K.W. Kim, J.H. Ahn, K.K. Cho, G.B. Cho, T.H. Nam, I.S. Ahn, H.J. Ahn, J. Alloys Compd. 449 (2008) 304–307.
[2] X. Zhu, Z. Wen, Z. Gu, S. Huang, J. Electrochem. Soc. 153 (2006) A504–A507.
[3] D.A.J. Rand, R. Woods, R.M. Dell, Batteries for Electric Vehicles, Research Studies Press Ltd., Taunton, Somerset, England, John Wiley & Sons Inc., New York, Chichester, Toronto, Brisbane, Singapore, 1998, pp. 483–529.
[4] N. Sato, J. Power Sources 99 (2001) 70–77.
[5] A. Taniguchi, N. Fujioka, M. Ikoma, A. Ohta, J. Power Sources 100 (2001) 117–124.
[6] K. Smith, C.Y. Wang, J. Power Sources 160 (2006) 662–673.
[7] K. Zaghib, P. Carest, A. Guerfi, J. Shim, M. Perrier, K. Striebel, J. Power Sources 134 (2004) 124–129.
[8] J. Prakash, L. Redey, D.R. Vissers, J. Power Sources 87 (2000) 195–200.
[9] R. Okuyama, J. Nakashima, T. Sano, E. Nomura, J. Power Sources 97 (2001) 50–54.
[10] J. Wang, J. Yang, Y. Nuli, R. Holze, Electrochem. Commun. 9 (2007) 31–34.
[11] C.W. Park, H.S. Ryu, K.W. Kim, J.H. Ahn, J.Y. Lee, H.J. Ahn, J. Power Sources 165 (2007) 450–454.
[12] C.W. Park, J.H. Ahn, H.S. Ryu, K.W. Kim, H.J. Ahn, Electrochem. Solid State Lett. 9 (2006) A123–A125.
[13] L.X. Yuan, J.K. Feng, X.P. Ai, Y.L. Cao, S.L. Chen, H.X. Yang, Electrochem. Commun. 8 (2006) 610–614.
[14] J.S. Kim, H.J. Ahn, H.S. Ryu, D.J. Kim, G.B. Cho, K.W. Kim, T.H. Nam, J.H. Ahn, J. Power Sources 178 (2008) 852–856.
[15] T.B. Kim, J.W. Choi, H.S. Ryu, G.B. Cho, K.W. Kim, J.H. Ahn, K.K. Cho, H.J. Ahn, J. Power Sources 174 (2007) 1275–1278.